

THE PENNSYLVANIA STATE UNIVERSITY
SCHREYER HONORS COLLEGE

DEPARTMENT OF BIOCHEMISTRY AND MOLECULAR BIOLOGY

CHARACTERIZATION OF PAD4 INHIBITION AND ITS ANTI-CANCER EFFECTS VIA
mTOR PATHWAY

HAONAN XU
SUMMER 2018

A thesis
submitted in partial fulfillment
of the requirements
for a baccalaureate degree
in Chemical Engineering
with honors in Biochemistry and Molecular Biology

Reviewed and approved* by the following:

Yanming Wang
Associate Professor, Biochemistry and Molecular Biology
Thesis Supervisor

Joseph Reese
Professor, Biochemistry and Molecular Biology
Honors Adviser

Wendy Hanna-Rose
Interim Department Head, Biochemistry and Molecular Biology
Department Reviewer

* Signatures are on file in the Schreyer Honors College.

ABSTRACT

PAD4 belongs to a family of enzymes that converts arginine and monomethyl arginine into citrulline. Citrullination of histone molecules can cause various transcriptional modulations, and the overexpression of PAD4 in neutrophil has been linked to many diseases. In the case of cancer, it was shown that inhibition of PAD4 can induce ER stress, trigger autophagy, and cause cancer cell death. In this study, two in-house PAD4 inhibitors GSK484-07 and YW4-03 have demonstrated potent effects on killing triple negative breast cancer cells. The treatments led to an upregulation of SESN2 signal, which suggests possible relation to mTOR mediated autophagy. Furthermore, YW4-03 was shown to increase HO-1 expression, which is indicative of oxidative stress. To further understand the anticancer mechanisms in which PAD4 is involved in, a CRISPR/Cas9 based human PAD4 knockout construct was created, despite the limited success in generating single colony knockout cell lines.

TABLE OF CONTENTS

LIST OF FIGURES	iv
LIST OF TABLES	v
ACKNOWLEDGEMENTS	vi
Chapter 1 Introduction	1
1.1 Chromatin Structure and Histone Modifications	1
1.2 PAD4	4
1.3 Neutrophil	5
1.4 mTOR Pathway	7
1.5 PAD Inhibitors	9
Chapter 2 Characterization of PAD4 Inhibition by GSK 484-07 and YW4-03	11
2.1 GSK 484-07 and YW4-03 Inhibits Cancer Growth in vitro	11
2.2 GSK484-07 and YW4-03 Activates SESN2	12
2.3 YW4-03 Activates HO-1	15
Chapter 3 Generation of PAD4 Knockout Cell Lines	17
3.1 CRISPR Construct Design	17
3.2 CRISPR Construct Verifications	19
3.3 Transfection and Unsuccessful Knockout Result	21
Chapter 4 Conclusion and Future Work	22
Chapter 5 Material and Methods	24
5.1 Cell Culture and Cryogenic Storage	24
5.2 MTT Assay	24
5.3 qRT-PCR and qPCR	25
5.4 Protein Sample Preparation	26
5.5 SDS-PAGE Gel	26
5.6 Western Blot	27
5.7 CRISPR Knockout	28
Appendix A Oligonucleotides and Primers Used	35
Appendix B Antibodies Used	36
Appendix C Buffer and Medium Recipes	37

Appendix D CRISPR Construct Design 39

Appendix E Abbreviations Used 41

BIBLIOGRAPHY 42

LIST OF FIGURES

Figure 1. Eukaryotic DNA Structure ³	2
Figure 2. Illustration of Histone Modifications ¹	3
Figure 3. Citrullination of Arginine by PAD Family Enzymes ⁸	4
Figure 4. Neutrophil Extracellular Trap (NET) Formation Pathways ⁴⁵	7
Figure 5. mTOR Repression Induced by ER Stress (Adapted ³² and Modified ³³⁻³⁴).....	8
Figure 6. Inhibition Curves of MDA-MB-231 Cell.....	11
Figure 7. Western Blot of SESN2 and p70S6K Signals under Inhibitor Treatments	13
Figure 8. mRNA levels of CHOP (a) and SESN2 (b) under PAD4 Inhibitor Treatments	14
Figure 9. Western Blot of PERK and HO-1 Signals under Inhibitor Treatments.....	16
Figure 10. Sequence Annotation of pSpCas9(BB)-2A-Puro (PX459) V2.0 Editing Site.....	18
Figure 11. Agarose Gel Image of CRISPR Plasmids Digested with Bbs I and Not I.....	19
Figure 12. Sequencing Results of CRISPR/Cas9 Constructs.....	20
Figure 13. Western Blot of Potential CRISPR Knockout Cells.....	21
Figure 14. Proposed Mechanisms for YW4-03.....	23
Figure 15. RT-PCR Run Method	25

LIST OF TABLES

Table 1. A List of PAD Inhibitors Used in this Study	10
Table 2. Reaction Conditions of sgRNA Oligonucleotides Annealing.....	28
Table 3. Reaction Conditions of Digestion/Ligation	29
Table 4. Reaction Conditions of De-Phosphorylation	30
Table 5. Reaction Conditions of Digestion-Based Construct Verification	31
Table 6. Complexation Components Preparation for MCF7 Transfection	32
Table 7. Complexation Components Preparation for HL-60 Transfection.....	33

ACKNOWLEDGEMENTS

First of all, I want to thank my principle investigator Dr. Yanming Wang, and PhD candidate Mr. Lai Shi for their mentorship over the last two years. Their guidance was irreplaceable during my time conducting research at South Frear.

I would also like to acknowledge the contributions from Dr. Gong Chen's group for synthesizing the inhibitors needed for the experiments, and Dr. Frank Pugh's group for the sharing of equipment.

Lastly, I would like to thank Dr. Joseph Reese from the Department of Biochemistry and Molecular Biology, Dr. Andrew Zydney, Dr. Ali Borhan, Dr. Darrell Velegol, and Dr. Wayne Curtis from the Department of Chemical Engineering, and Dr. William Noid from the Department of Chemistry, for their support and guidance during my professional career at Penn State.

Chapter 1

Introduction

1.1 Chromatin Structure and Histone Modifications

Eukaryotic DNA is found in a highly-structured nucleoprotein complex called chromatin^{2,7-9}. The basic chromatin building block is the nucleosome, which contains 147 bp of DNA wrapped around a histone core octamer (two of each histones H2A, H2B, H3, and H4) for 1.65 turns^{2,9}. Each nucleosome is further stabilized by a linker histone H1 molecule while connecting to others with a segment of DNA^{2,9}. The nucleosomes are then folded into 30 nm fibers, 250 nm fibers, and eventually a chromatid³ (Fig. 1). This ordered assembly is essential for packaging a large amount of genetic material in limited nucleus space; and it further creates spatial constraints that act as an additional layer of gene activation control¹⁻². Namely, transcriptional machineries require sufficient space to access DNA, and nucleosomal assembly occupies those binding sites⁴. Compared to heterochromatin, or the tightly packed chromosomal regions, euchromatin is loosely packed, more accessible, and contains most of genes¹.

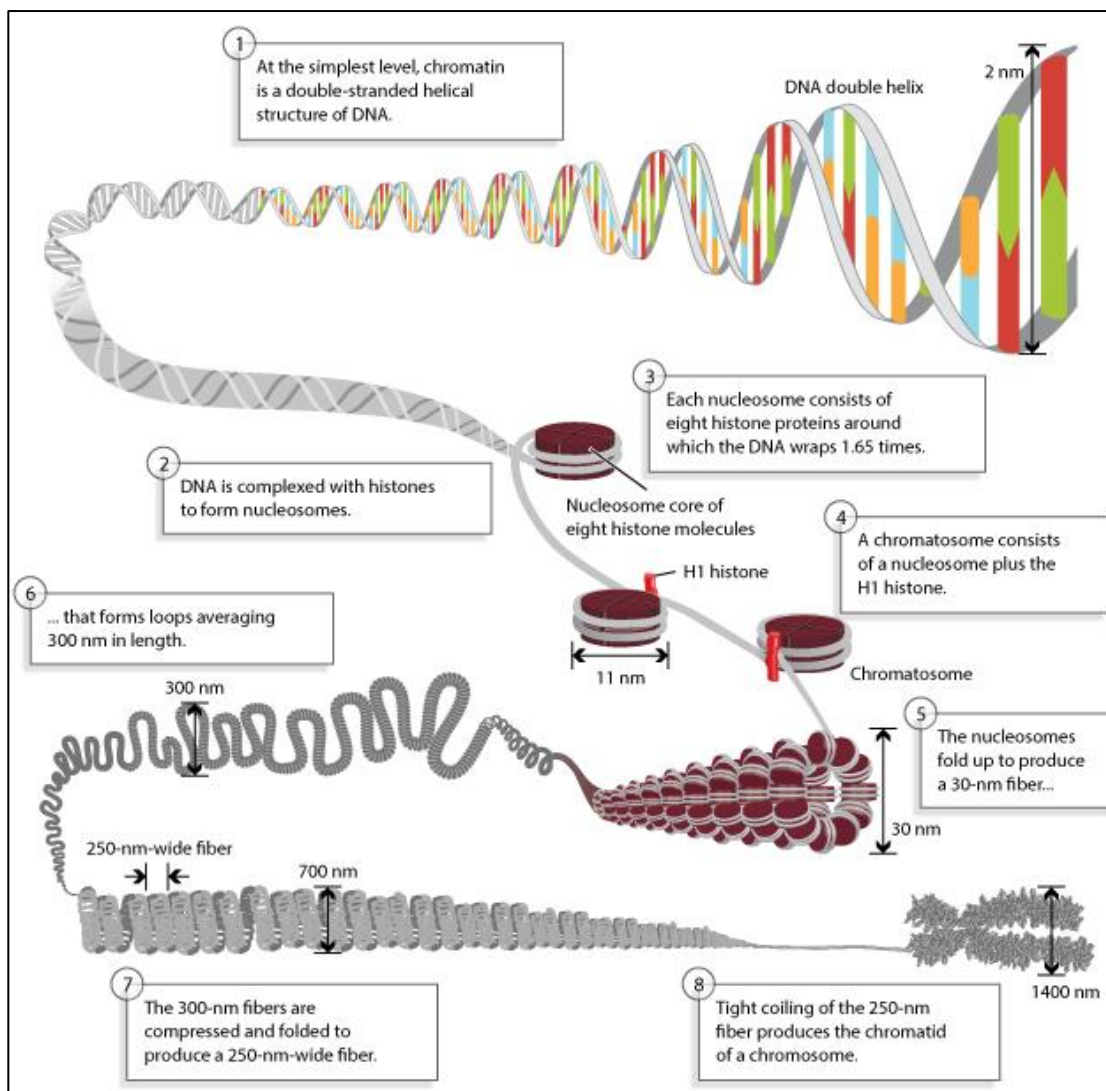


Figure 1. Eukaryotic DNA Structure³

Eukaryotic DNA is organized into nucleosomes. Nucleosomes are further packed into higher order structures to condense into the limited space for DNA storage. This organization also imposes another level of gene regulation, which is subject to epigenetic modifications. This figure was reprinted from the work of Annunziato while complying with the terms of use³.

Additionally, a series of histone post translational modifications (PTMs) can modulate the activation and repression of genes^{1, 7-9} (Fig. 2). The structural evidence indicates that histone N-terminal tail interacts with neighboring nucleosome, and covalent modifications on the tail can affect the inter-nucleosomal interaction, and leads to chromosome structure changes⁹. PTMs can

lift the spatial constraint on transcription, such as H3K4me3 marking euchromatin and promoting transcriptional elongation; PTMs can also have repressive effects, like H3K27me3 silencing transcription and causing X-inactivation^{5,9}. Furthermore, modifications of histone globular domain are also frequently observed although not as well understood. H3K79 methylation in yeast telomere silencing is a well-known example⁵. Besides methylation, additional modifications such as acetylation, phosphorylation, and mono-ubiquitination are all well documented^{1,5}. While many PTMs participate in gene regulation, there are also others fulfilling structural functions, or serving as inheritable epigenetic markers^{1,4}.

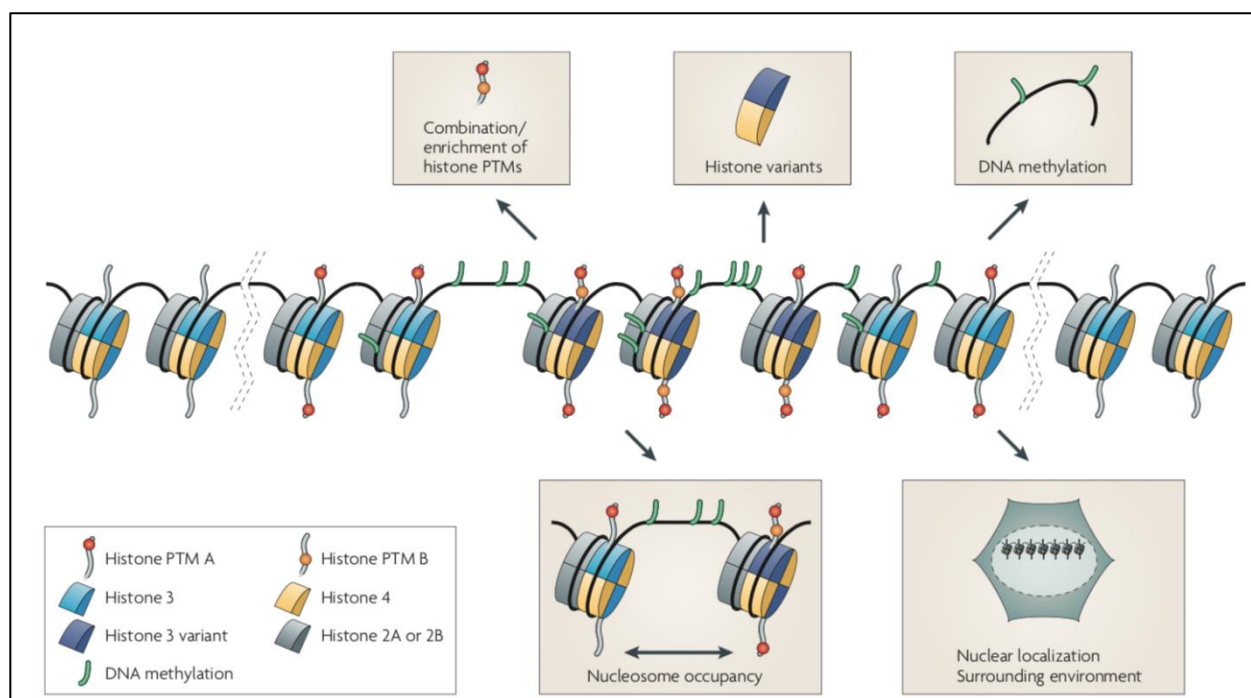


Figure 2. Illustration of Histone Modifications ¹

Epigenetic modifications can involve covalent changes to both DNA and histones. In histone molecule, post-translational modifications can occur on globular domains, as well as histone tails. These PTMs can regulate gene expressions, fulfill structural roles, and transmit inheritable epigenetic information. This figure was reprinted from the work of Margueron and Reinberg with permission¹.

1.2 PAD4

In addition to the aforementioned PTMs, there are also other modifications that are emerging as key regulators of transcriptions and diseases. Citrullination catalyzed by protein arginine deiminase 4 (PAD4) is one of them (Fig. 3). Up until the discovery of the first histone demethylase in 2004, the methylation modification was considered relatively stable, with the exception of PADs catalyzed demethylation process by converting methylated arginine residue into citrulline residue⁹⁻¹⁰.

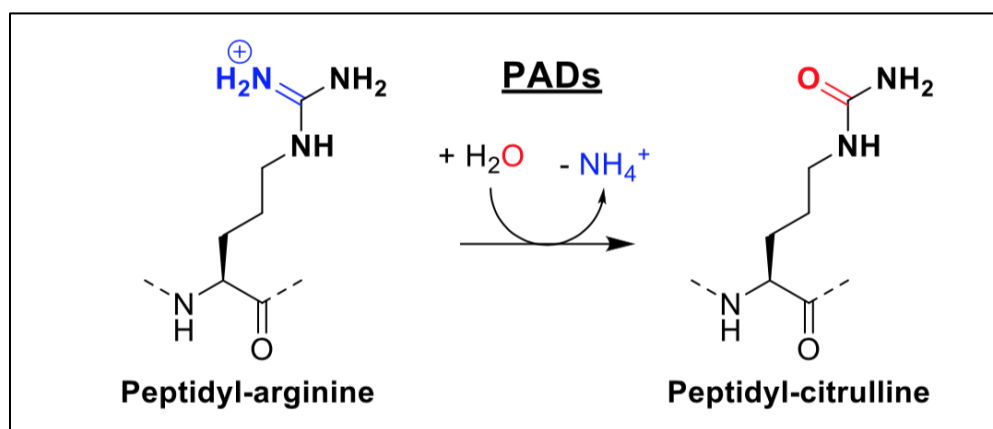


Figure 3. Citrullination of Arginine by PAD Family Enzymes⁸

PAD family enzymes hydrolyze peptidyl-arginine molecules to produce peptidyl-citrulline. Citrullination has been shown as a functional epigenetic modification that is linked to various diseases. This figure was reprinted from the work of Fuhrmann and Thompson with permission⁸. Figure license requests should be directed to *ACS Chemical Biology*.

Although PAD2 has been shown to reside in the nucleus, PAD4 is the only member of the PAD family (PAD1-4, and 6) that contains a canonical nuclear localization signal^{10-11,13}. Interestingly, unlike most of histone modification enzymes that act in a sequence dependent manner, PAD4 recognizes a highly disordered conformation, which allows it to target multiple

arginine/monomethyl arginine sites with low sequence specificity¹⁰. Citrullination reaction also effectively replaces the positively charged guanidinium group with a neutral urea group, therefore leading to possible chromatin structure change and downstream gene regulation¹⁰. Both activating and repressing transcriptional effects have been reported for citrullination²⁸.

In terms of stem cell maintenance, the chromatin decondensation as a result of histone H1R54Cit has been linked to the activation of various pluripotency genes¹²⁻¹³. In the case of cancer, evidence shows citrullination activity is negatively correlated to tumor size in a p53 dependent manner²⁵. In fact, PAD4 was shown to be a co-repressor of p53 where it cooperates with histone deacetylase HDAC2 to silence key tumor suppressor genes like p21 and GADD45²⁵⁻²⁷. Furthermore, PAD4 has been linked a variety of diseases for its abnormally enhanced expression in neutrophils, including rheumatoid arthritis (RA), multiple sclerosis, systemic lupus erythematosus (SLE), cancer and its associated conditions (i.e. thrombosis, renal insufficiency, etc.)¹⁴⁻²⁰.

1.3 Neutrophil

Besides pathogenesis through direct gene suppression (i.e. p53 silencing), PAD4's overexpression can also trigger diseases involving neutrophil and autoimmune reactions⁴³. Neutrophil is the most abundant type of leukocytes in blood and an essential part of innate immune system against bacterial infections²¹⁻²³. Three methods of pathogen killing response have been documented for neutrophils, phagocytosis, or the engulfment of foreign microbes, degranulation of cytotoxic enzymes, and NETosis²⁰. NETosis is a self-sacrificing defense mechanism where neutrophil releases DNA mesh and cytotoxic enzymes to trap foreign

microbes through one of the two pathways depicted in Fig. 4^{20-23,45}. Furthermore, neutrophil has a very short circulating half-life of 6 to 8 hours, which requires rapid turnover⁴⁴. While abundance and efficacy of neutrophils make them irreplaceable defenders against pathogens, the anomalous occurrence of NETs has been associated to serious diseases including SLE, thrombosis, cancer related renal dysfunction, and secondary metastasis¹⁶⁻²⁰. PAD4 is known to be essential for the neutrophil extracellular trap (NET) formation^{22,24}, therefore both Pan-PAD (i.e. Cl-amidine, YW3-56) and PAD4 specific inhibitors (i.e. GSK 484) were developed and tested as potential therapeutics for these diseases^{18,20,24,33}. While there still needs to be more comprehensive understandings prior to clinical applications, the current results are generally positive^{18,20,24,33}. However, one of the more significant risks is the danger of neutropenia, where the neutrophil number is severely low²⁰. Many chemotherapy drugs can already cause neutropenia, and any further PAD inhibitions can amplify the risk of infection²⁰.

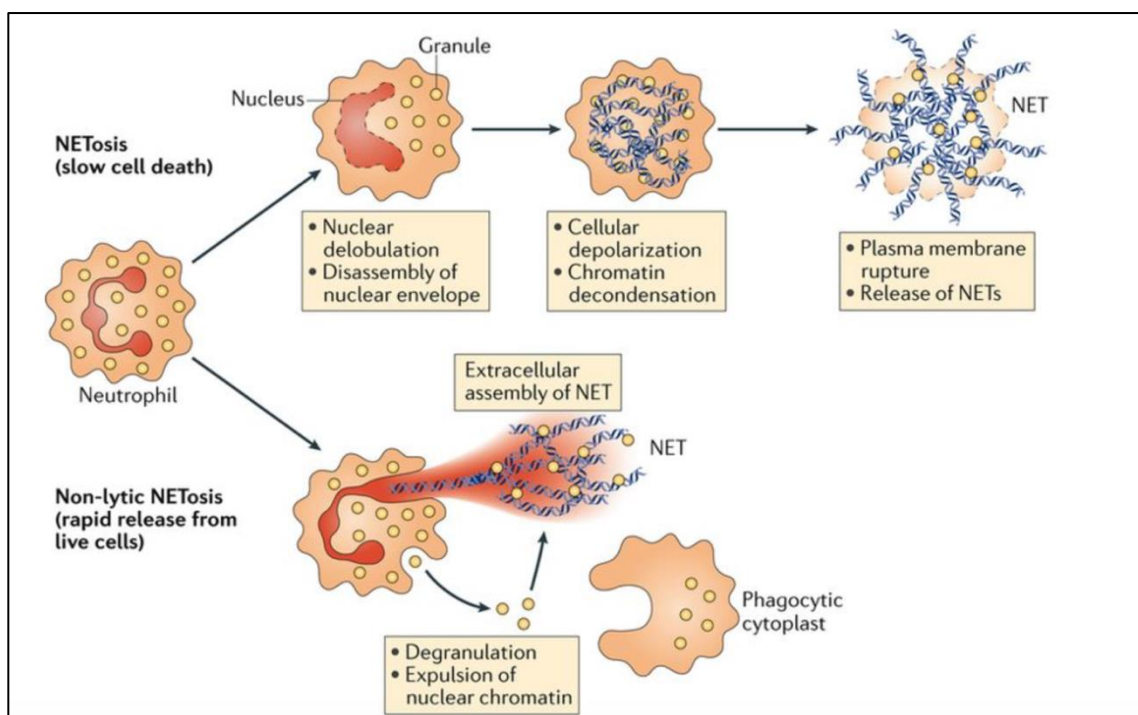


Figure 4. Neutrophil Extracellular Trap (NET) Formation Pathways⁴⁵

Neutrophil can undergo NETosis through two pathways, lytic and non-lytic. In the case of non-lytic NETosis, chromatin and cytotoxic enzymes are assembled extracellularly. This figure was reprinted from the work of Papayannopoulos with permission⁴⁵.

1.4 mTOR Pathway

PAD4 inhibitors like YW3-56 exhibited cancer killing effect by triggering macroautophagy through the mTOR pathway³³. In addition to well-known apoptosis, or programmed cell death, macroautophagy (hereafter referred to as autophagy) is another self-destructive process. During autophagy, portions of cytoplasmic organelles are sequestered within double- or multi-membraned autophagosomes, and the autophagosomes are then fused with lysosomes for mass degradation²⁹⁻³⁰. Mammalian target of rapamycin (mTOR) kinase is a critical control point against autophagy process²⁹⁻³⁰. Two p53 target genes sestrin1 (SESN1) and sestrin2

(SESN2) were shown to promote autophagy by indirectly inhibiting mTOR through the activation of AMPK³⁰⁻³¹ (Fig. 5). Induction of endoplasmic reticulum (ER) stress also activates SESN2 as an endogenous mTOR inhibitor in an activating transcription factor 4 (ATF4) mediated fashion, which eventually leads to autophagy³²⁻³³. In the case of p53 as a modulator, although p53 activates pro-autophagy genes like SESN2, accumulated cytoplasmic p53 can inhibit autophagy through unknown mechanisms³⁰. Competent p53 was reported to be essential for SESN2's function as a positive autophagy regulator³⁰, although conflicting result was also documented³³.

Various PAD inhibitors generated by our group have shown promising anti-cancer properties through in vitro studies, and the inhibition of mTOR pathway is one of the proposed mechanisms^{26, 33}.

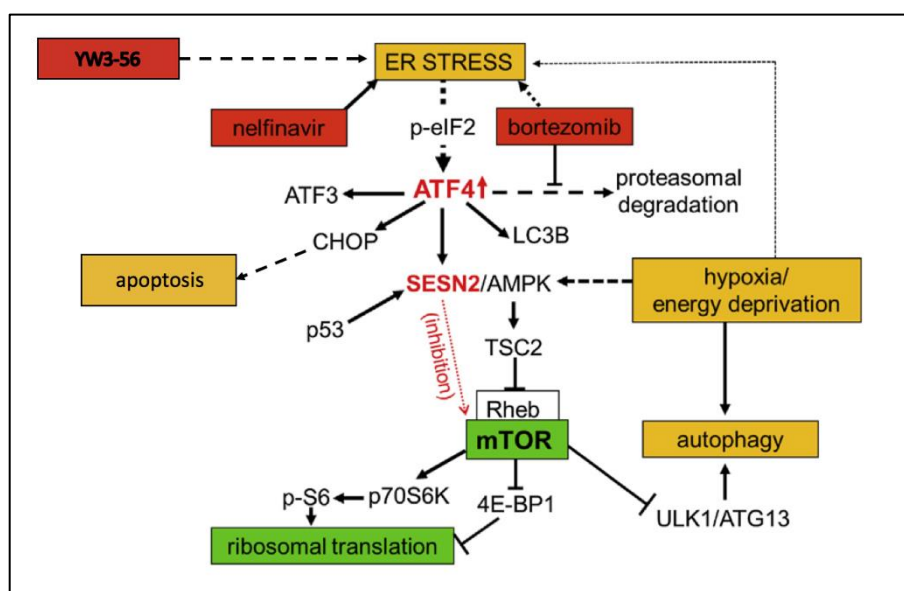


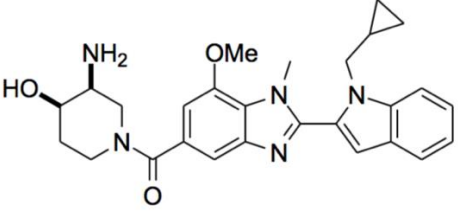
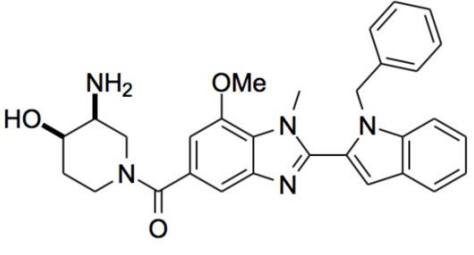
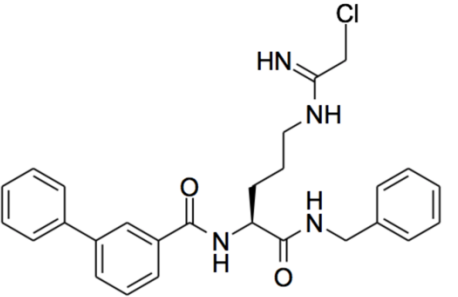
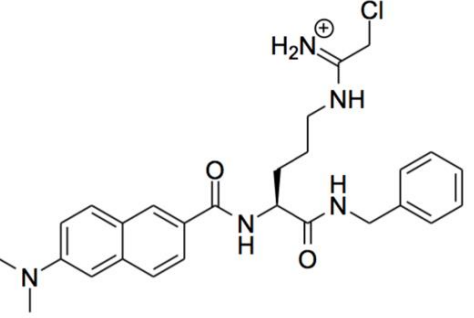
Figure 5. mTOR Repression Induced by ER Stress (Adapted³² and Modified³³⁻³⁴)

Nelfinavir and Bortezomib are anticancer drugs currently in clinical trials, they have been shown to upregulate ATF4 as a part of ER stress response that leads to autophagy. It was further demonstrated that PAD4 inhibitor YW3-56 can also trigger autophagy involving the same ATF4-SESN2-mTOR signaling axis. This figure was adapted from the work of Brüning and colleagues³², and further modified based on the work of Wang, Tabas, and colleagues³³⁻³⁴.

1.5 PAD Inhibitors

F-amidine and Cl-amidine were the first characterized PAD inhibitors^{24, 28}, however, these inhibitors can only interact with Ca²⁺ ion bound form of PAD4. They irreversibly inactivate the enzyme by covalently modifying Cys645²⁸. Within the cellular environment, the Ca²⁺ ion availability is regulated by transmembrane protein calcium ionophore, therefore PAD4 is not always in Ca²⁺ bound form, and there are needs for calcium ion independent inhibitors²⁸. Small molecule library screening led by Lewis and colleagues showed GSK 484 as a potent citrullination and NETs inhibitor, and it has strong preference of PAD4 over other PAD enzymes as well as negligible off-target activity²⁴. In collaboration with Professor Gong Chen's group (Department of Chemistry, Penn State), our group generated various medicinal chemistry alterations of the compound GSK484. GSK484-07 is used in this study for its excelled potency. Furthermore, YW4-03 and YW3-56 are among the list of Pan-PAD inhibitors developed by our group. While YW3-56 was shown to trigger ER stress and subsequent mTOR signaling, little is known about the effects of GSK484-07 and YW4-03^{26, 33} (Table 1).

Table 1. A List of PAD Inhibitors Used in this Study

Compound Name	Compound Structure	Literature Comments
GSK 484		IC ₅₀ : PAD4 = 250 nm (2 mM Ca ²⁺) IC ₅₀ : PAD4 = 50 nm (0 mM Ca ²⁺) ^{8, 24}
GSK 484-07 (a GSK 484 derivative)		N/A
YW4-03 (Pan PAD Inhibitor)		IC ₅₀ : PAD4 = ~5 μM IC ₅₀ : Cell Growth = 2.5-5 μM ²⁶ Reduction of Tumor size in mouse ³⁵
YW3-56 (Pan PAD Inhibitor)		IC ₅₀ : PAD4 = 1-5 μM IC ₅₀ : Cell Growth = ~ 2.5 μM ²⁶

Chapter 2

Characterization of PAD4 Inhibition by GSK 484-07 and YW4-03

2.1 GSK 484-07 and YW4-03 Inhibits Cancer Growth in vitro

GSK 484-07 and YW4-03 are two in-house inhibitors manufactured by our collaborators. Inhibition of cancer cell growth was characterized using the MTT colorimetric assay. Tetrazolium salt MTT (3-(4,5-dimethylthiazol-2-yl)-2,5-diphenyl tetrazolium bromide) is a substrate that can be reduced by mitochondrial enzymes to produce a bright purple colored product³⁶. Since only live cells can carry out the reduction, an inhibitor concentration dependent killing curve can be generated. The two inhibitors were tested on triple negative breast cancer cell line MDA-MB-231 (Fig. 6).

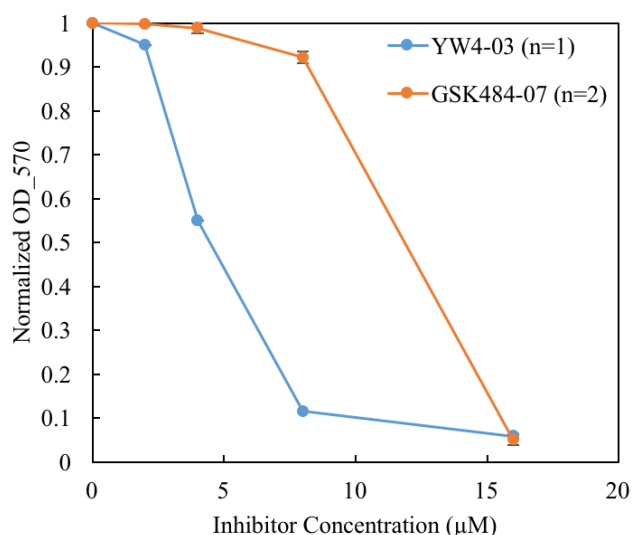


Figure 6. Inhibition Curves of MDA-MB-231 Cell

Killing curve was generated using MTT assays. Error bar shown for the GSK484-07 is the standard deviation of two independent repeats. The inhibitors were incubated with cells for 48 hours.

While both inhibitors demonstrated significant efficacies on restricting cancer cell growth (<15 μM), YW4-03 was shown to be a more potent compound.

2.2 GSK484-07 and YW4-03 Activates SESN2

Wang and colleagues demonstrated that YW3-56 can activate ATF4 and upregulate the expression of mTOR inhibitory gene SESN2³³, which subsequently prevents ribosomal translation and triggers autophagy³²⁻³³. Here, the structurally similar molecule YW4-03 was evaluated for its potential effects in the same pathway. Western blot data (Fig. 7) indicate that YW4-03 does activate SESN2 at the IC_{50} of 5 μM , and ImageJ quantification shows an over 20-fold increase when compared to DMSO control; although it is not as potent as YW3-56, which exhibits an over 35-fold enhancement. The SESN2 signal at 10 μM of YW4-03 was not further intensified, likely caused by high ratios of cell detachment and death.

Furthermore, when treated with YW3-56, SESN2 downstream target 70 kDa ribosomal S6 kinase (p70S6K) exhibits reduced phosphorylation at threonine 389 residue³³. Despite the poor purity of this particular antibody, this p-Thr389 reduction is visible when compared to DMSO control (Fig. 7). However, the same reduction was not observed for YW4-03 or GSK484-07 treatments. Independent repeat did not show p-Thr389 reduction neither, and it is not yet clear if YW4-03 functions through a different mechanism. Furthermore, the antibody used for p70S6K p-T389 detection (9205S, CST) can also detect p85S6K p-Thr412 where the phosphorylation is analogous³⁷. Clear bands at around 85 kDa were observed indeed. Interestingly, p85S6K phosphorylation is also subject to inhibitor treatment, and it closely resembles the trend of p70S6K p-T389 changes.

Moreover, it was observed that at elevated level of YW4-03 ($2\times IC_{50}$), cellular concentration of p70S6K protein was reduced. While it is possible that cellular toxicity restricts ribosomal function and reduces protein production, it could also be caused by the faster degradation of p70S6K protein comparing to the loading control of histone H3 due to its larger size. The p70S6K band migration for GSK484-07 treatment (Fig.7 Lane 4) deviated slightly comparing to others of the same gel, this can only be attributed to the inhomogeneity of polyacrylamide gel casted, and it presents no significant influence on characterizing p70S6K expression.

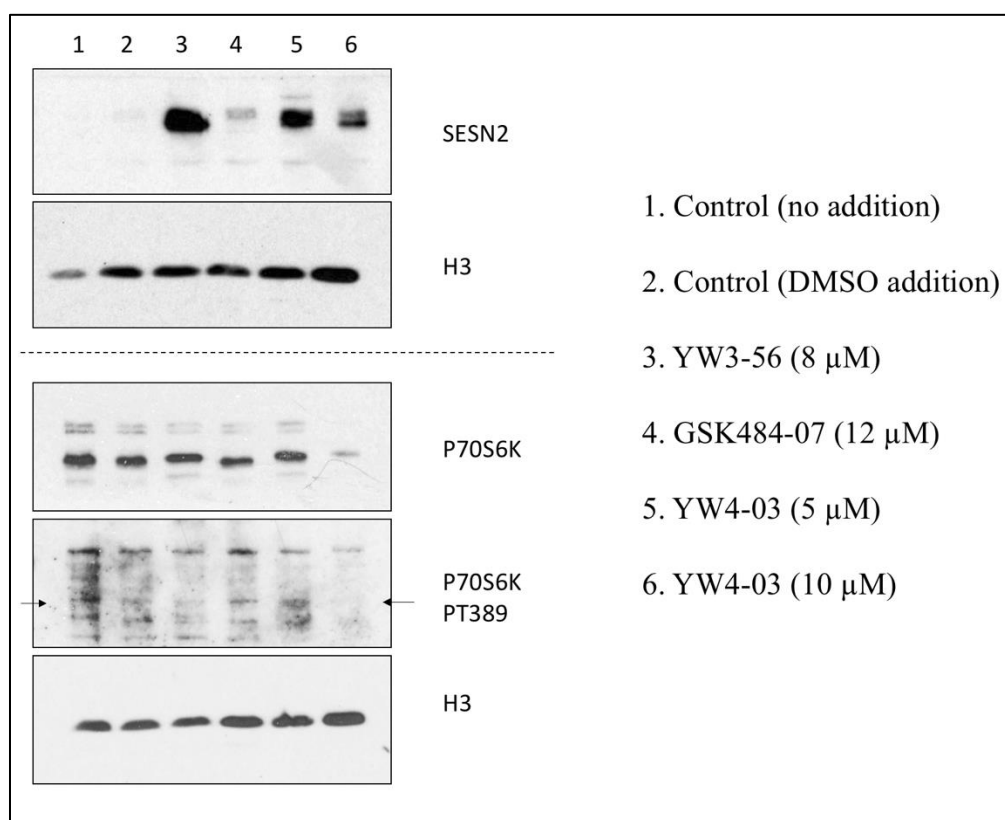


Figure 7. Western Blot of SESN2 and p70S6K Signals under Inhibitor Treatments

Western blot data show enhanced SESN2 expression for YW3-56, GSK484-07, and YW4-03 treatments. However, the p70S6K Thr389 phosphorylation was only reduced for YW3-56 treatment. H3 was used as a loading control.

Surprisingly, the enhancement of SESN2 at protein level was not correlated to any variations at the mRNA level. Quantitative PCR (qPCR) study found no significant changes ($p>0.2$) between control groups and PAD4 inhibitor treatment groups on CHOP and SESN2 mRNA level (Fig. 8). Transcription factor C/EBP homologous protein (CHOP, also known as DDIT3 or GADD153) is a key component of ER stress mediated apoptosis pathway⁴⁶. It is in parallel to SESN2 under ATF4 activation (Fig. 5)³³⁻³⁴. While western blot data for CHOP is not conclusive, qPCR data suggests its mRNA level is well maintained for MDA-MB-231 cell line during YW4-03 and GSK484-07 treatments. Furthermore, it is not yet clear how SESN2 mRNA levels showed no significant change in response to YW4-03 treatments while protein levels enhanced drastically. Further studies are needed to address this discrepancy.

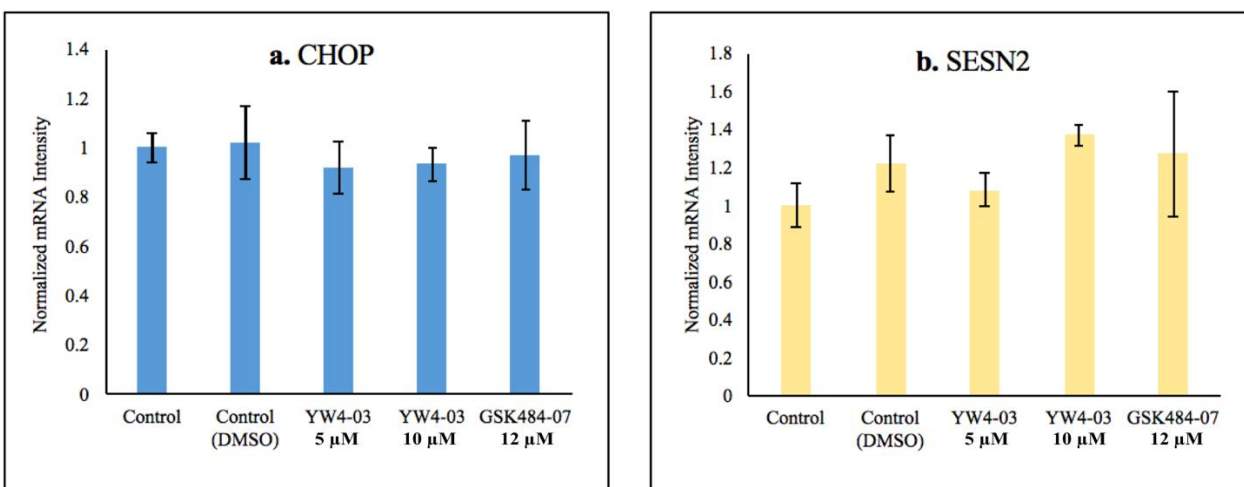


Figure 8. mRNA levels of CHOP (a) and SESN2 (b) under PAD4 Inhibitor Treatments

The mRNA levels were normalized against control for each of the target molecule. The y-axis is the mRNA expression level relative to the control group, a value greater than 1 suggests the particular treatment enhances the target molecule transcription; a value less than 1 suggests the transcription is repressed; and a value equal to 1 suggests the inhibitor treatment has no effects on the target mRNA. DMSO control was added to account for any transcriptional modulations caused by the DMSO solvent that inhibitors are dissolved in. The error bar is the standard deviation of internal repeats. **(a)** CHOP signal change was not significant across the board. **(b)** SESN2 mRNA level did not change when

compared to control group, however, doubling IC₅₀ marginally increased SESN2 transcription (p = 0.018).

Functionally speaking, YW4-03 and GSK484-07 enhance the SESN2 protein expression. Since SESN2 is a key regulator of the mTOR signaling pathway, the downstream influence of these inhibitors can be inferred. Although current data are inconclusive in demonstrating the relationship between the cancer cell killing effect and autophagy activation, they are sufficient in presenting YW4-03 and GSK484-07 as plausible research targets.

The exact mechanisms of cancer inhibition and how PAD4 fits in them are still unclear. A PAD4 knockout cell line is needed to further evaluate the functionality of these PAD4 inhibitors.

2.3 YW4-03 Activates HO-1

In addition to mTOR signaling involvements, oxidative stress was also detected for YW4-03 treatments. Heme oxygenase-1 (HO-1) is a cytoprotective and anti-inflammatory enzyme that can be induced in response to oxidative stress⁴⁰. Induced HO-1 expression can cause HO-1 protein to translocate to mitochondria and lead to mitochondrial dysfunction under normoxic conditions, as opposed to the protective effects under the normal endoplasmic reticulum (ER) associated state⁴¹. Furthermore, YW3-56 mediated cell death involves mitochondria depletion based on transmission electron microscopy images³³. There is no evidence to suggest that the mitochondria depletion observed is linked to the induced expression of HO-1. However, YW4-03 does enhance HO-1 expression (Fig. 9), which is a definitive sign

of oxidative stress, and it can lead to mitochondrial depletion⁴¹. GSK484-07 treatment does not exhibit nearly as significant HO-1 upregulation as YW4-03.

Furthermore, protein kinase R-like endoplasmic reticulum kinase (PERK) has been shown as an upstream regulator of HO-1⁴². Despite the significant elevation in HO-1, the modulation in PERK protein level is negligible.

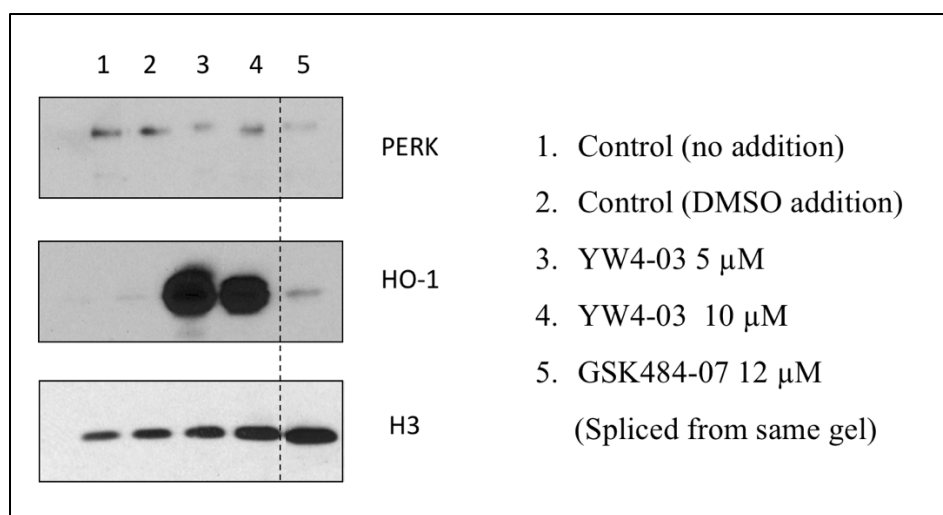


Figure 9. Western Blot of PERK and HO-1 Signals under Inhibitor Treatments

Western blot data show enhanced HO-1 signals for YW4-03 treatments, while GSK484-07 does not exhibit the same sign of oxidative stress. H3 was used as a loading control.

It is not yet clear where HO-1 upregulation fits in the mechanisms of PAD4 inhibition mediated cancer cell killings, although the oxidative stress induction would further expand the potential drug effectors of YW4-03.

Chapter 3

Generation of PAD4 Knockout Cell Lines

3.1 CRISPR Construct Design

Although various PAD4 and Pan PAD inhibitors have demonstrated efficacies towards cancer inhibition, there is a lack of clear understanding on where PAD4 fits in the pathway of autophagy or alternative cell death mechanisms. Currently, correlations to at least two pathways have been demonstrated. One, PAD4 inhibition upregulates p53, which enhances SESN2 and AMPK signals, and triggers downstream autophagy²⁵⁻²⁷; and two, PAD4 inhibition upregulates ATF4, which enhances SESN2 and AMPK signals, and triggers downstream autophagy and mitochondria depletion³³⁻³⁴. While it is more than likely that the two pathways coexist, it is beneficial from the pharmacological development standpoint to identify which of the two pathways takes precedent.

Moreover, the MDA-MB-231 cell line used in this study has a gain-of-function mutant p53 that can elevate survival signals via phospholipase D when deprived of serum³⁸. Therefore, alternative cell lines should be used to carry out unbiased studies. p53 wild type human breast cancer cell line MCF7 and p53-null human acute promyelocytic leukemia cell line HL-60 were selected as targets for PAD4 knockout.

Based on the protocol and supplemental CRISPR Design software published by Ran and colleagues, a CRISPR sgRNA was generated to target the Exon 1 of PAD4 (Appendix A)³⁹. The design software identified 27 additional off-target sites for this construct, however, this particular

sg DNA is the optimal option. A commercial CRISPR/Cas9 plasmid *pSpCas9(BB)-2A-Puro (PX459) V2.0* was used to transiently express the genome editing machineries needed for introducing double stranded breaks. Insertion-Deletion (Indel) mutations were expected for the non-homologous end joining (NHEJ) repairs that cells would carry out to repair breaks.

Conveniently, the plasmid construct contains BbsI restriction sites leading to gRNA scaffold (Fig. 10). Since the two restriction site overhangs are non-complementary, a single-tube digestion/ligation was carried out instead of traditional gel extraction process.

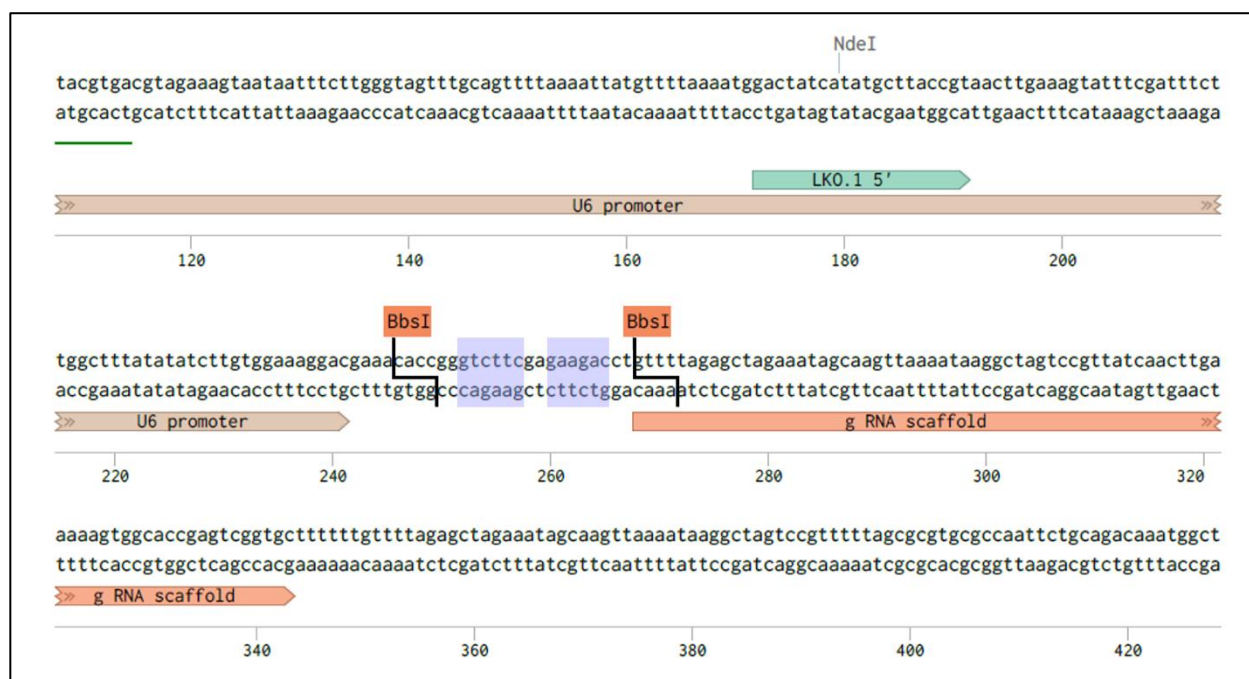


Figure 10. Sequence Annotation of pSpCas9(BB)-2A-Puro (PX459) V2.0 Editing Site

The recognition sequences for BbsI restriction enzyme are highlighted in purple. The cutting sites are labelled using black lines. LKO. 1 5' shown in green is the sequencing primer. This figure was generated using the Benchling software.

3.2 CRISPR Construct Verifications

The ligated construct was then transformed into DH5-alpha competent cell and selected using ampicillin resistance. The PX459 plasmid contains an ampicillin resistance selectable marker, and the survival of colonies in LB Amp+ plates is indicative of successful transformation. However, colony survival does not distinguish the sg DNA incorporated edits from unmodified constructs. A digestion based verification is needed to eliminate false positive colonies. A group of colonies were each expended in liquid medium; their plasmids were subsequently extracted and double digested with Bbs I and Not I restriction enzymes. The PX459 has two BbsI restriction sites that would be deleted upon sg DNA insertion, where the NotI restriction site is unaffected. Therefore, a single band at 9 kb indicates no BbsI cutting, which is consistent with the sg DNA ligated construct. The unedited PX459 plasmids should exhibit two bands at 3kb and 6kb, and the third fragment is too small to be detected on the 1% agarose gel.

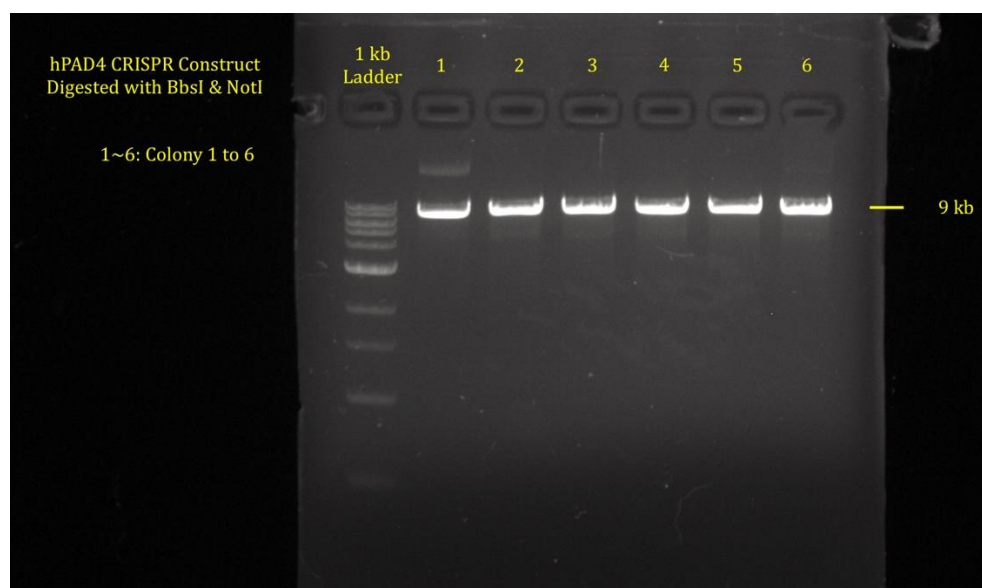


Figure 11. Agarose Gel Image of CRISPR Plasmids Digested with Bbs I and Not I

CRISPR sg DNA inserted plasmids were double digested with restriction enzymes Bbs I (cuts at +246 and +268) and Not I (cuts at +6431). Only sg DNA modified constructs were detected among the 6 plasmid samples. The electrophoresis was done using a 1% agarose gel.

Based on the digestion results (Fig. 11), colonies 2 through 5 were selected as possible PAD4 sg DNA constructs. Colony 1 plasmid digest has an additional band that is greater than 10 kb; it is likely an open circular form of edited plasmid caused by Not I partial digestion. The plasmids from the colony 2 to colony 5 were sequenced for confirmation. Colony 2, 4, and 5 plasmids have the most definitive reads (Fig. 12), and are used for downstream transfection. The sequencing results of CRISPR colonies are aligned to the theoretical construct design. The omission of the adenine is likely due to the close proximity of reading site to sequencing primer, which is only 44 base pairs away. The other ambiguity occurs within the gRNA scaffold. Both inconsistencies are within the PX459 backbone, and are unlikely to be the results of ligation.

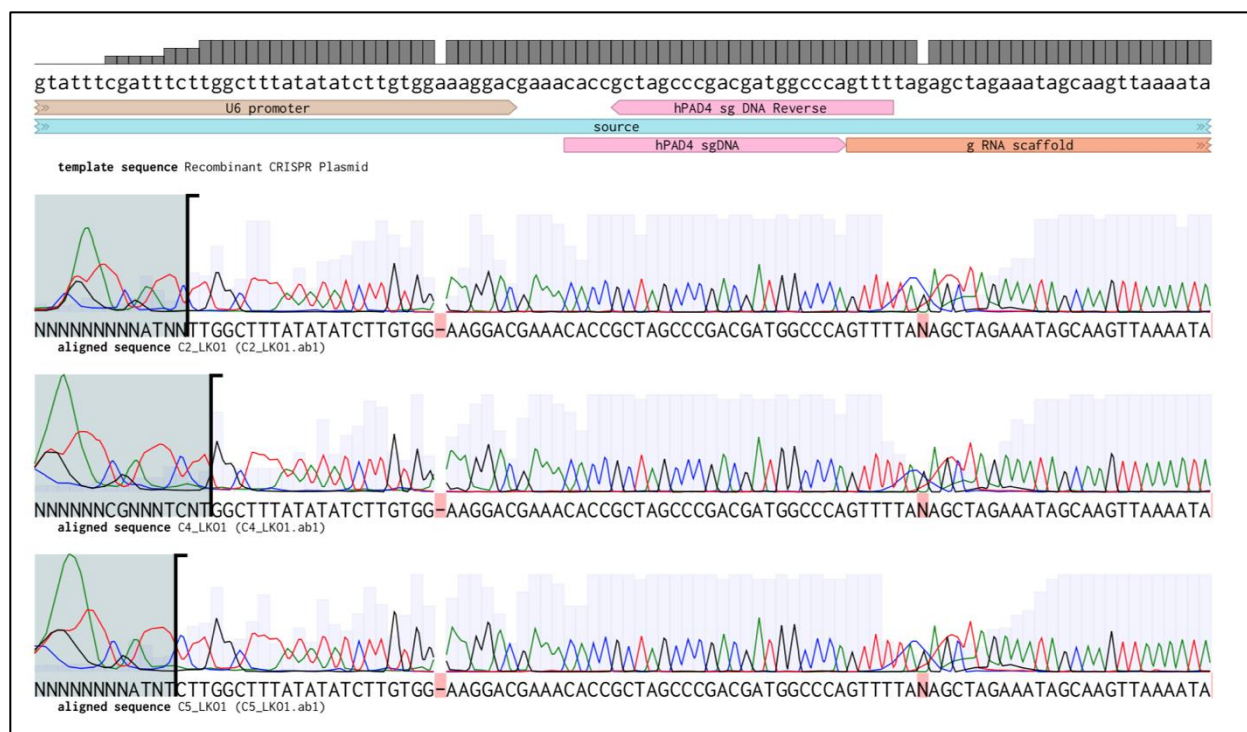


Figure 12. Sequencing Results of CRISPR/Cas9 Constructs

The sequences of colonies 2, 4, and 5 are aligned against the theoretical sg DNA containing construct. The PAD4 sg DNA for both plus and minus strands are shown in pink, and their overhangs are in complementary to those of the backbone. PX459 sequence used for the virtual sg DNA insertion is from the supplier's website. This figure was generated using the Benchling software.

3.3 Transfection and Unsuccessful Knockout Result

Transfection and puromycin selection have proven to be difficult to achieve. Cell survival post transfection was extremely low. Both manual dilution and flow cytometry based single cell sorting were used in attempt to isolate single cell colonies. For HL-60 cells, it was also particularly challenging to assess the colony development due to its flotation nature. For MCF7 cells, only one colony was identified from over 500 samples. This single colony was gradually expanded, and screened for PAD4 knockout result. Anti-PAD4 antibody was an in-house product, and even with its lack of specificity, the consistency with the positive control suggests that PAD4 knockout was not achieved (Fig. 13). This attempt at generating human PAD4 knockout cell line will be repeated in the future.

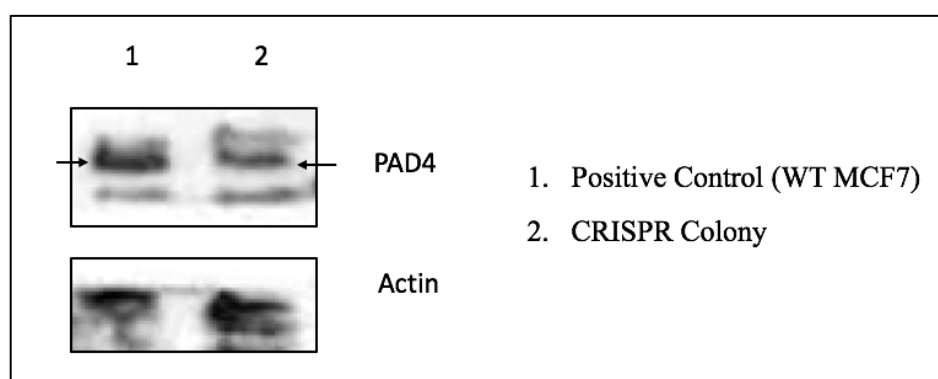


Figure 13. Western Blot of Potential CRISPR Knockout Cells

In-house PAD4 antibody was used to detect the PAD4 expression of the MCF7 CRISPR Colony. Wild type MCF7 cells cultured in the same conditions were used as the positive control. Actin was used as a loading control.

Chapter 4

Conclusion and Future Work

The cancer inhibition effects of YW4-03 and GSK484-07 on MDA-MB-231 have been demonstrated using MTT assay. Since their structurally similar counterparts YW3-56 and GSK484 modulate autophagy flux, it was plausible that YW4-03 and GSK484-07 may also play a role in regulating the mTOR signaling pathway leading to autophagy. Unlike the negligible mRNA changes shown by qPCR, western blot data demonstrated that YW4-03 and GSK484-07 do enhance the protein expression of SESN2, which is a key regulator of mTOR. However, the SESN2 downstream target p70S6K Thr389 phosphorylation data were not as conclusive as that of YW3-56 treatment's. Furthermore, HO-1 protein expression was drastically enhanced with the addition of YW4-03, which indicates oxidative stress. Based on the data shown in this thesis, as well as literature references, plausible mechanisms for YW4-03 mediated cancer killing are proposed (Fig. 14). Most notably, the hypothesized model for YW4-03 involves both apoptosis and autophagy mediated by ER and mitochondrial oxidative stress. YW4-03 activation of SESN2 and HO-1 were demonstrated in this thesis, and all other pathway components are based on literature data of PAD4 inhibition and mTOR signaling^{32-34, 42}. Since GSK484-07 does not show oxidative stress marker HO-1, the parameters for its mechanism is not yet clearly defined. Additional research is needed to verify the exact nature of both YW4-03 and GSK484-07 based cancer killings.

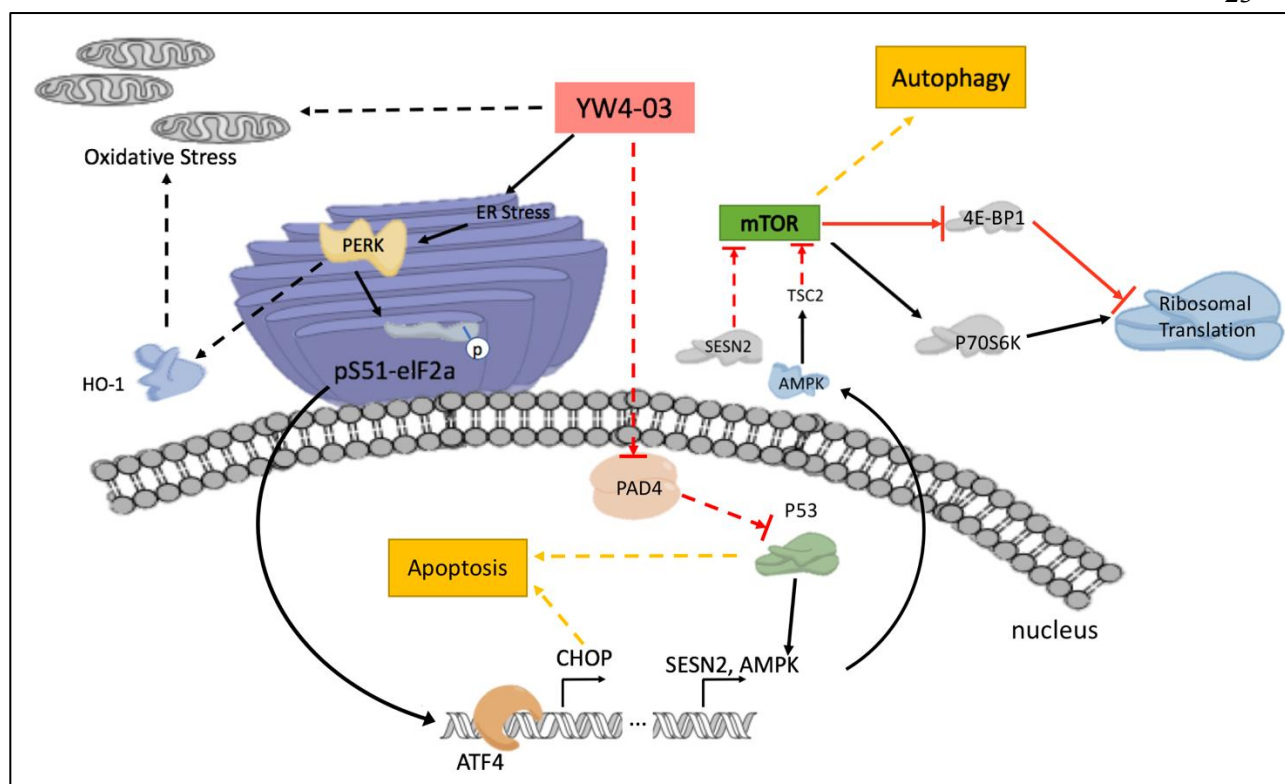


Figure 14. Proposed Mechanisms for YW4-03

The proposed YW4-03 cancer inhibition mechanisms involve both autophagy and apoptosis pathways. Downregulations are shown in red arrow, and upregulations are in black arrow. This figure was generated using ChemDraw[®] software.

To establish the exact placement of PAD4 in autophagy regulation, a CRISPR/Cas9 based knockout construct was also generated and sequence verified. However, it had been challenging to create a monoclonal knockout colony using puromycin selectable marker. Future attempts could involve fluorescence based constructs to reduce selection toxicity. Obtaining human PAD4^{-/-} cancer cell lines would expand the understanding of specific pharmacological basis of PAD4 inhibitions in clinical setting. Future work should focus on generating a PAD4 knockout cell line, as well as validating the proposed mechanisms for YW4-03 by characterizing the expression levels of key intermediate components shown in Fig. 14.

Chapter 5

Material and Methods

5.1 Cell Culture and Cryogenic Storage

MDA-MB-231 and HL-60 cells were cultured in DMEM Medium (Gibco) supplemented with 10% v/v FBS and 1% v/v PS. MCF7 and MIA PaCa-2 cells were cultured in RPMI Medium (1640, Gibco) with the same supplements. Cells were incubated at 37 °C with 5% CO₂, and passaged when confluent. Cryogenic stocks are made with 50% v/v Trypsin-free fresh medium, 40% FBS, and 10% DMSO.

5.2 MTT Assay

Inhibitors were added at 80% cell confluency for 48-hour incubation. MTT was then added to the cells (at 0.5 mg/mL) for two-hour incubation. Upon completion, medium was aspirated, and DMSO was added to dissolve the cell membrane. The samples were agitated for 5 minutes in dark, prior than reading at 570 nm absorbance. In the event of floating cells, samples were transferred to Eppendorf tubes and pelleted (Centrifuge 5415 D, Eppendorf) before the medium removal.

5.3 qRT-PCR and qPCR

Cells were cultured and treated in 6 well plates. The culture was washed using PBS, and the total RNA was harvested using the PureLink™ RNA Mini Kit (Invitrogen) according to the manufacturer's instructions. The RNA purity and concentration was assessed using a spectrophotometer (ND-1000, NanoDrop®). Quantitative reverse transcription PCR (qRT-PCR) was done using qScript™ cDNA SuperMix (Quanta BioSciences) following manufacturer's instructions. Quantitative PCR (qPCR) of specific gene was performed using PerfeCTa® SYBR Green SuperMix (Quanta BioSciences) in StepOnePlus Real-Time PCR System (Applied Biosystems). The reaction mixture consists of 2 µL of 2.5 µM RT-PCR Primer, 2 µL of cDNA (1ng/µL), 2 µL of water, and 6 µL of SuperMix. The specific run method is shown in the Figure 15. A list of primers used for qPCR is shown in the Appendix A.

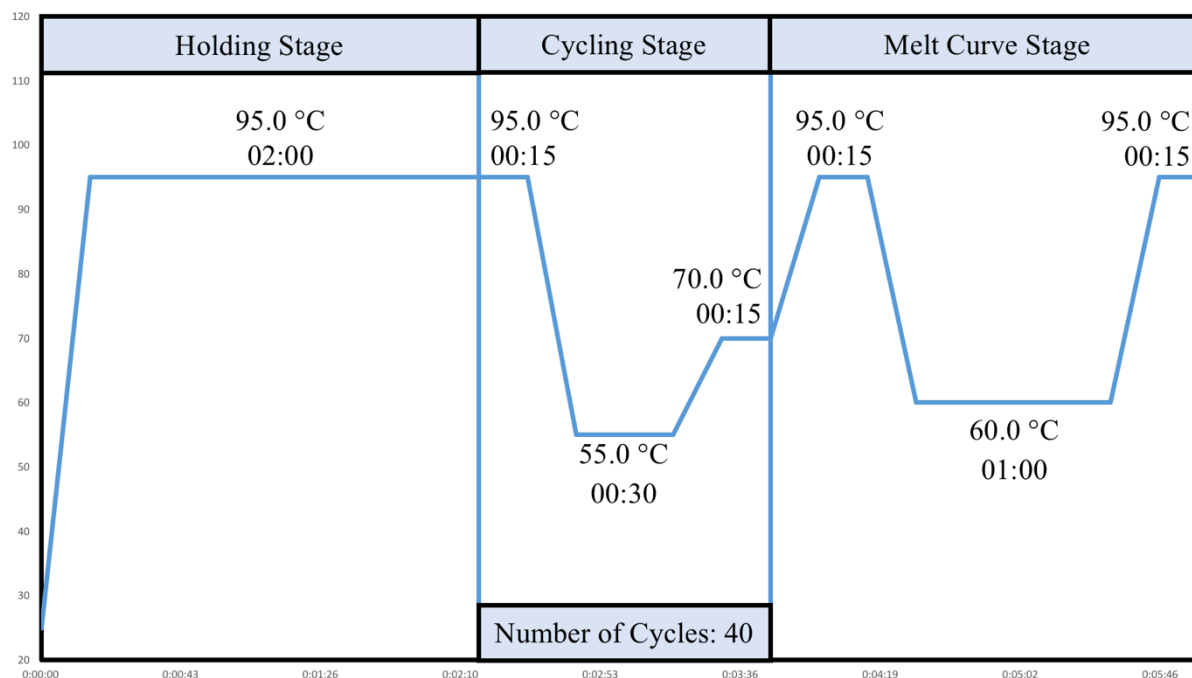


Figure 15. RT-PCR Run Method

SYBR Green was used as an intercalating dye for all qPCR experiments. qPCR runs were performed in three stages with the cycling stage repeated for a total of 40 times. Data were then exported from the Applied Biosystems software, and interpreted in Microsoft Excel.

5.4 Protein Sample Preparation

Cells were cultured and treated in 6 well plates. After desired time of incubation, cells were washed with PBS, then trypsinized (0.05% Trypsin-EDTA, Glibco[®]) prior than counting using a hemocytometer. Cells were then pelleted at 4 °C at 132000 RPM (Centrifuge 5415D, Eppendorf) for 5 minutes. Supernatant was discarded, and cells were resuspended in PBS. The pelleting process was repeated to remove trace medium and trypsin. Cell pellets were resuspended in ice chilled IP buffer with protease inhibitors (PMSF at 10 µg/µL; pepstatin A, leupeptin, and aprotinin at 1 µg/µL) at the ratio of 100 µL/million cells. The suspension was then sonicated on low setting for 15 min (Bioruptor[®], Diagenode Diagnostics). Protein samples were stored at -20 °C.

5.5 SDS-PAGE Gel

Equalized protein samples were mixed with 6x Loading Buffer and water to achieve a final concentration of 1x Loading Buffer. The prepared protein loading samples were denatured (>80 °C for 5 minutes) and loaded on the gel along with protein ladder (Crystalgen). Adjacent wells on each side were flanked with equal volume of 1x SDS loading buffer to ensure straight protein migration. Polyacrylamide Gel (13% running, 4% stacking) was run in the Running Buffer at 230 V until the dye front has exited the gel.

5.6 Western Blot

Following polyacrylamide gel electrophoresis, the stacking portion was separated and discarded. Proteins were then transferred onto nitrocellulose membrane (BioTrace™ NT Nitrocellulose Transfer Membrane, Pall Laboratory) using semi-dry transfer method (TE 77 ECL Semi-Dry Transfer Unit, Amersham Biosciences) at constant current of 99 mA for 1 hour. Transfer Buffer was used to soak filter papers, membrane, and gel. Upon transfer, membrane was then stained with Ponceau S dye (0.1% w/v Ponceau S in 5% v/v acetic acid, Sigma) and destained with deionized water to reveal protein bands. Targeted protein bands along with loading controls were cut out and washed using TBST buffer for three times, 10 minutes each. Primary antibodies were diluted in 5% BSA at the appropriate concentrations. Protein membranes were then incubated in primary antibody (Rotator, Glas-Col®) overnight at 4 °C. Post incubation, the membranes were washed using TBST (3 times, 10 minutes each) to remove non-specific binding. The membranes were then incubated with appropriate secondary antibody conjugated with HRP in BSA solution for 2 hours at 4 °C. The washing process was repeated before HRP substrates (VisiGlo™ Select HRP Chemiluminescent Substrate Kit, VWR) were added. Finally, the protein signal was blotted onto autoradiography films (HyBlot CL®, Denville Scientific) in dark room, then developed using a film processor (SRX-101A, Konica; CBM-20 Chemical Mixing Station, ChemBlend). A list of antibodies used for western blot is shown in the Appendix B.

5.7 CRISPR Knockout

The CRISPR/Cas9 construct was designed and generated based on the work of Ran and colleagues³⁹. The detailed procedures are listed below^{39,51}.

Designing of Cas 9 Guide RNA

PAD4 knockout construct sg DNA design was generated using CRISPR design software made by Feng Zhang group³⁹. The PAD4 exon 1 sequence was obtained from NCBI⁴⁹ and manually inputted as the target. The optimal oligonucleotides were selected based on the least amount of off-targets. Oligonucleotides were then ordered from IDT[®].

Annealing the sg DNA Oligonucleotides

The two oligonucleotides were annealed at the conditions shown in the Table 2. Upon completion, the annealed sg DNA product was diluted 200 folds.

Table 2. Reaction Conditions of sgRNA Oligonucleotides Annealing

Reaction Mixture Composition	
Components	Amount (μ L)
sgRNA Coding Strand (100 μ M)	1
sgRNA Non-coding Strand (100 μ M)	1
T4 PNK Buffer, 10X	1
T4 Polynucleotide Kinase (PNK)	1
Water (Molecular Biology Grade)	6
Total	10

Thermocycler Setting	
Temperature (°C)	Time (min)
37	30
95	5
Ramp down to 25	5 °C/ min

Digestion and Ligation

The one pot digestion/ligation reaction was done following the conditions listed in the Table 3.

Table 3. Reaction Conditions of Digestion/Ligation

Reaction Mixture Composition	
Components	Amount
pSpCas9(BB)-2A-Puro-(PX459) V2.0	100 ng
Diluted oligonucleotides (annealed)	6 µL
Fastdigest Buffer, 10X	1 µL
Fastdigest BbsI	1 µL
T4 Ligase	0.5 µL
Water (Molecular Biology Grade)	(to 20 µL)
Total	20 µL
Thermocycler Setting	
Temperature (°C)	Time (min)
37	5
21	5
Repeat for 6 times	

De-phosphorylation

De-phosphorylation reaction was done to deactivate any linear PX459 plasmids following the conditions listed in the Table 4.

Table 4. Reaction Conditions of De-Phosphorylation

Reaction Mixture Composition	
Components	Amount
Ligation Product	10
Antarctic Phosphatase (5 U/mL)	1
Antarctic Buffer, 10x	1.5
Water (Molecular Biology Grade)	2.5
Total	15
Thermocycler Setting	
Temperature (°C)	Time (min)
37	15
70	5

Heat shock Transformation

DH5-Alpha competent cell (20 μ L) was mixed with de-phosphorylated product (3 μ L). The mixture was incubated on ice for 30 minutes, then immediately transferred to a 42 °C heat block for 90 seconds. Upon completion, the mixture was placed back on ice for additional 5-minute incubation. LB medium (200 μ L, antibiotic free) was added to the

competent cell/DNA mixture. The culture was incubated for 30 minutes (37 °C, 180 RPM), and plated (100 µL) on LB agar with ampicillin (100 µg/mL) for selection.

Plasmid Extraction

After overnight incubation at 37 °C, colonies were picked and inoculated into liquid LB medium (2 mL, with ampicillin at 100 µg/mL) for 9 hours. The cells were harvested, and the plasmid DNA was extracted using EZNA[®] Plasmid DNA Mini Kit following manufacturer's instructions.

Digestion-Based Construct Verification

The extracted plasmid was digested using Not I and Bbs I following the conditions shown in the Table 5.

Table 5. Reaction Conditions of Digestion-Based Construct Verification

Reaction Mixture Composition	
Components	Amount (µL)
Plasmid (50 ng/uL)	2
BbsI (NEB)	0.5
NotI	0.5
NEB Buffer 2.1	1
Water (Molecular Biology Grade)	6
Total	10
Thermocycler Setting	
Temperature (°C)	Time (min)
37	30

A 37 °C incubator was used instead of thermocycler. Upon completion, the digested plasmids were run on a 1% agarose gel. Plasmids that exhibit a single 9kb band are consistent with sg DNA incorporated CRISPR/Cas9 construct, and were sent for sequencing.

Sequencing

Sequencing was done by the Penn State Nucleic Acid Facility. LKO.1 5' was used as the sequencing primer. Sequence verified plasmids were used for transfecting the MCF7 cells and HL-60 cells.

Transfection

Lipofectamine™ 3000 kit (ThermoFisher) was used following the manufacturer's instructions⁴⁷⁻⁴⁸. MCF7 cells were seeded in RPMI medium in a 24 well plate (1.1×10^5 cells in 500 μ L) and allowed to grow to 70% confluency overnight. At the time of transfection, complexation components are prepared as shown in Table 6.

Table 6. Complexation Components Preparation for MCF7 Transfection

Tube	Complexation Components	Amount per well (24-well)
Tube 1	Opi-MEM I Medium	25 μ L
	Lipofectamine 3000 reagent	1 μ L
Tube 2	Opti-MEM I Medium	25 μ L
	DNA (at concentration of 0.5-5 μ g/ μ L)	250 ng
	P3000™ reagent	0.5 μ L

The tube 2 components were then added to the tube 1 and mixed. The entire mixture was allowed to incubate at room temperature for 10 minutes before adding to the cells.

The HL-60 cells were transfected following the generic protocol⁴⁸. The key difference is that two LipofectamineTM 3000 reagent volumes were attempted at once (Table 7).

Table 7. Complexation Components Preparation for HL-60 Transfection

Tube	Complexation Components	Amount per well (24-well)
Tube 1.1 & Tube 1.2	Opi-MEM TM Medium	25 μ L x 2 tubes
	Lipofectamine 3000 reagent	0.75 μ L and 1.5 μ L
Tube 2	Opi-MEM TM Medium	50 μ L
	DNA (at concentration of 0.5-5 μ g/ μ L)	1 μ g
	P3000 TM reagent	2 μ L

25 μ L of the tube 2 mixtures were added to each of the Tube 1s. The final mixtures were incubated for 10 minutes at room temperature before adding to 2 separate wells of cells.

Selection

Puromycin was initially used to select the transfection at 2 μ g/mL, and the medium was refreshed after 24-hour treatment. Due to the large proportions of cell death, the puromycin selection pressure was reduced to 1 μ g/mL, and the incubation time was increased to more than two weeks⁵⁰.

Single Cell Dilution

In order to generate monoclonal colonies, the cells were seeded in 96 well plates at the ratio of one cell per well. Two approaches were employed, manual dilution and flow cytometry based cell sorting. For manual dilution, the selected cells were counted using a hemocytometer, then diluted down to 1 cell/100 μ L. While there was no guarantee that each well would have only one cell, the statistical likelihood for having at least one monoclonal colony was high. For flow cytometry based cell sorting, the sorting was done by the Penn State Microscopy & Cytometry Facility (37 °C, 100- μ m injection tip, MoFlo Astrios, Beckman Coulter). The plates from both methods were closely monitored. No colony was found in the flow cytometry sorted groups; the cells are likely to be damaged by shear stress.

Appendix A

Oligonucleotides and Primers Used

qPCR Primers

Target	Forward	Reverse
Actin	5' -AGAGCTACGAGCTGCCTGAC-3'	5' -AGCACTGTGTTGGCGTACAG-3'
DDIT3	5' -CGCCTGACCAGGGAAGTAGA-3'	5' -TCATGCTTGGTGCAGATTCAC-3'
SESN2	5' -AATACCATCGCCATGCACAGT-3'	5' -ATGCCAAAGACGCAGTGGAT-3'

Sequencing Primer

LKO.1 5'	5' -GACTATCATATGCTTACCGT-3'
----------	-----------------------------

Oligo Fragments

CRISPR	5' -CACCGCTAGCCCGACGATGGCCCA-3'
sgRNA	3' -CGATCGGGCTGCTACCGGGTCAAA-5'

Appendix B

Antibodies Used

Primary Antibody

Antigen	Catalog Number	Manufacturer	Source	Antigen Size	Dilution
a-Tubulin	T6199	Sigma-Aldrich	Mouse	50 kDa	1:8000
DDIT3	SC7351	Santa Cruz Biotechnology	Mouse	29 kDa	1:400
H3	Ab1791	Abcam	Rabbit	15 kDa	1:5000
HO-1	10701-1-AP	Proteintech	Rabbit	33 kDa	1:3000
PERK (C33E10)	#3192S	Cell Signaling Technology	Rabbit	140 kDa	1:1000
p70 S6 Kinase	9202S	Cell Signaling Technology	Rabbit	70, 85 kDa	1:1000
Phospho-p70 S6 Kinase (Thr389)	9205S	Cell Signaling Technology	Rabbit	70, 85 kDa	1:1000
SESN2	Ab57810	Abcam	Mouse	54 kDa	1:2000
PAD4	n/a	(in house)	Rabbit	70 kDa	1:500

Secondary Antibody

Antibody	Catalog Number	Manufacturer	Source	Antigen Size	Dilution
Anti-M HRP	NA931	GE Healthcare	Sheep	n/a	1:2000
Anti-R HRP	NA934	GE Healthcare	Donkey	n/a	1:2000

Appendix C

Buffer and Medium Recipes

IP Buffer

20mM Tris-HCl, pH8.0,

150mM NaCl,

10mM EDTA,

0.2% Triton X-100,

0.2% NP-40

SDS loading buffer (6X)

300 mM Tris.HCl (pH6.8)

20% Glycerol

6% SDS

4% Beta - mercaptoethanol

0.6% Bromophenol

Running Buffer

25 mM Tris

190 mM glycine

0.1% SDS

Transfer Buffer

25 mM Tris

190 mM Glycine

10% Methanol

TBST

19 mM Tris•HCl

137 mM NaCl

2.7 mM KCl

Adjust pH to 7.4 via HCl

0.1% Tween 20

5% Blotto

5% w/v Non-fat dry milk powder in TBST

LB Medium (for 1 L)

10 g tryptone

5 g yeast extract

10 g NaCl

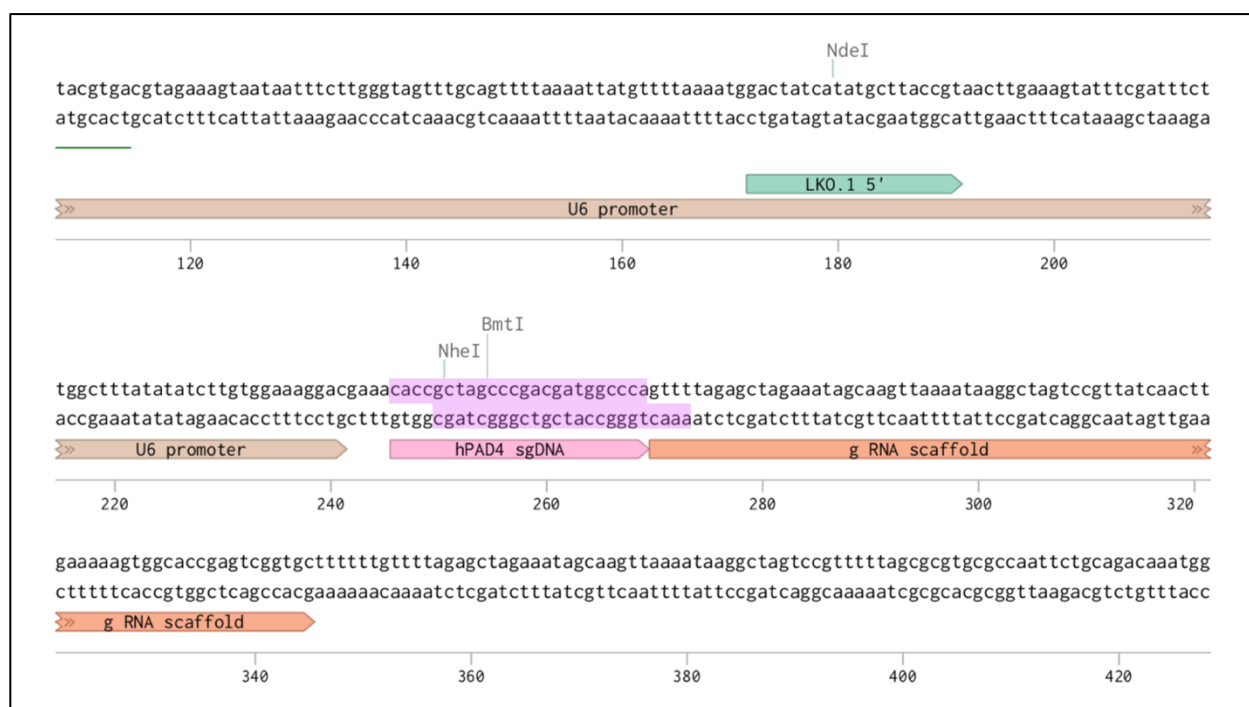
Adjust the pH to 7.0 with 1 N NaOH

Appendix D

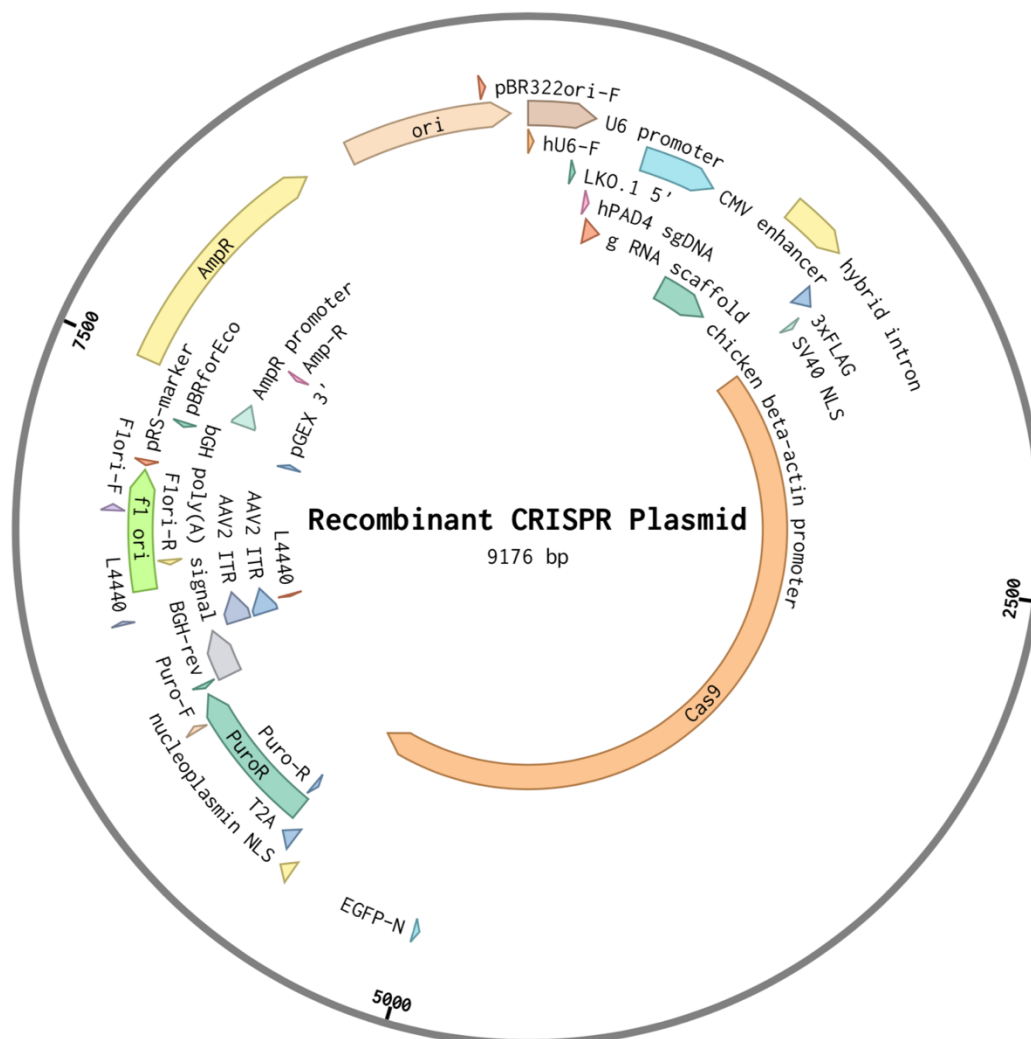
CRISPR Construct Design

(Figures were generated using the Benchling Software)

The ligated sg DNA sequence is shown below.



The complete sg DNA inserted construct map is shown below.



Appendix E

Abbreviations Used

Abbreviation	Meaning
4E-BP1	Eukaryotic translation initiation factor 4E binding protein 1
APMK	AMP-activated protein kinase
CHOP	C/EBP-homologous protein
DDIT3	DNA Damage Inducible Transcript 3
DDIT4	DNA Damage Inducible Transcript 4
DMEM	Dulbecco's Modified Eagle Medium
DMSO	Dimethyl sulfoxide
ER	endoplasmic reticulum
FBS	Fetal bovine serum
HO-1	Heme oxygenase-1
MTT	3-(4,5-Dimethylthiazol-2-yl)-2,5-Diphenyltetrazolium Bromide
P-P70S6K T389	70 kDa ribosomal S6 kinase phosphorylated at threonine 389
P70S6K	70 kDa ribosomal S6 kinase
PAD4	Protein Arginine Deiminases 4
PBS	Phosphate-buffered saline
PERK	protein kinase R-like endoplasmic reticulum kinase
PS	Penicillin-Streptomycin (10,000 U/mL)
pS51-eIF2a	Eukaryotic translation initiation factor 2 subunit 1 phosphorylated at serine 51
RPMI	Roswell Park Memorial Institute (RPMI) 1640 Medium
SDS	Sodium dodecyl sulfate
SDS-PAGE	sodium dodecyl sulfate polyacrylamide gel electrophoresis
SESN2	Sestrin 2
TBST	tris-buffered saline (TBS) with Tween 20
TEMED	Tetramethylethylenediamine
Tris	tris(hydroxymethyl)aminomethane
TSC2	Tuberous Sclerosis Complex 2

BIBLIOGRAPHY

1. Margueron, R. & Reinberg, D. Chromatin structure and the inheritance of epigenetic information. *Nature Reviews Genetics* **11**, 285–296 (2010).
2. Quina, A. S., Buschbeck, M. & Di Croce, L. Chromatin structure and epigenetics. *Biochemical Pharmacology* **72**, 1563–1569 (2006).
3. Annunziato, A. DNA Packaging: Nucleosomes and Chromatin. *Nature Education* **1**, 26 (2008).
4. Venkatesh, S. & Workman, J. L. Histone exchange, chromatin structure and the regulation of transcription. *Nature Reviews Molecular Cell Biology* **16**, 178–189 (2015).
5. Lawrence, M., Daujat, S. & Schneider, R. Lateral Thinking: How Histone Modifications Regulate Gene Expression. *Trends in Genetics* **32**, 42–56 (2016).
6. Budhavarapu, V. N., Chavez, M. & Tyler, J. K. How is epigenetic information maintained through DNA replication? *Epigenetics & Chromatin* **6**, 32 (2013).
7. Alberts, B. *et al.* *Molecular biology of the cell*. 196-198, (Garland Science Taylor & Francis, 2008).
8. Fuhrmann, J. & Thompson, P. R. Protein Arginine Methylation and Citrullination in Epigenetic Regulation. *ACS Chemical Biology* Available at <https://pubs.acs.org/doi/abs/10.1021/acscchembio.5b00942>, **11**, 654–668 (2015).
9. Bannister, A. J. & Kouzarides, T. Regulation of chromatin by histone modifications. *Cell Research* **21**, 381–395 (2011).

10. Arita, K. *et al.* Structural basis for histone N-terminal recognition by human peptidylarginine deiminase 4. *Proceedings of the National Academy of Sciences* **103**, 5291–5296 (2006).
11. Vossenaar, E. R., Zendman, A. J., Venrooij, W. J. V. & Pruijn, G. J. PAD, a growing family of citrullinating enzymes: genes, features and involvement in disease. *BioEssays* **25**, 1106–1118 (2003).
12. Slade, D. J., Subramanian, V. & Thompson, P. R. Citrullination unravels stem cells. *Nature Chemical Biology* **10**, 327–328 (2014).
13. Christophorou, M. A. *et al.* Citrullination regulates pluripotency and histone H1 binding to chromatin. *Nature* **507**, 104–108 (2014).
14. Jones, J. *et al.* Protein arginine deiminase 4 (PAD4): current understanding and future therapeutic potential. *Current opinion in drug discovery & development* **12**, 616–627 (2013).
15. Fan, L. *et al.* PADI4 Epigenetically Suppresses p21 Transcription and Inhibits Cell Apoptosis in Fibroblast-like Synoviocytes from Rheumatoid Arthritis Patients. *International Journal of Biological Sciences* **13**, 358–366 (2017).
16. Knight, J. S. *et al.* Peptidylarginine deiminase inhibition disrupts NET formation and protects against kidney, skin and vascular disease in lupus-prone MRL/lpr mice. *Annals of the Rheumatic Diseases* **74**, 2199–2206 (2015).
17. Wen, F., Shen, A., Choi, A., Gerner, E. W. & Shi, J. Extracellular DNA in Pancreatic Cancer Promotes Cell Invasion and Metastasis. *Cancer Research* **73**, 4256–4266 (2013).
18. Cedervall, J. *et al.* Pharmacological targeting of peptidylarginine deiminase 4 prevents cancer-associated kidney injury in mice. *OncImmunology* **6**, (2017).

19. Demers, M. *et al.* Cancers predispose neutrophils to release extracellular DNA traps that contribute to cancer-associated thrombosis. *Proceedings of the National Academy of Sciences* **109**, 13076–13081 (2012).
20. Park, J. *et al.* Cancer cells induce metastasis-supporting neutrophil extracellular DNA traps. *Science Translational Medicine* **8**, (2016).
21. Leshner, M. *et al.* PAD4 mediated histone hypercitrullination induces heterochromatin decondensation and chromatin unfolding to form neutrophil extracellular trap-like structures. *Frontiers in Immunology* **3**, (2012).
22. Li, P. *et al.* PAD4 is essential for antibacterial innate immunity mediated by neutrophil extracellular traps. *The Journal of Experimental Medicine* **207**, 1853–1862 (2010).
23. Fuchs, T. A. *et al.* Novel cell death program leads to neutrophil extracellular traps. *The Journal of Cell Biology* **176**, 231–241 (2007).
24. Lewis, H. D. *et al.* Inhibition of PAD4 activity is sufficient to disrupt mouse and human NET formation. *Nature Chemical Biology* **11**, 189–191 (2015).
25. Tanikawa, C. *et al.* Regulation of histone modification and chromatin structure by the p53–PADI4 pathway. *Nature Communications* **3**, 1–10 (2012).
26. Wang, Y. *et al.* Anticancer Peptidylarginine Deiminase (PAD) Inhibitors Regulate the Autophagy Flux and the Mammalian Target of Rapamycin Complex 1 Activity. *Journal of Biological Chemistry* **287**, 25941–25953 (2012).
27. Li, P. *et al.* Coordination of PAD4 and HDAC2 in the regulation of p53-target gene expression. *Oncogene* **29**, 3153–3162 (2010).
28. Luo, Y. *et al.* Inhibitors and Inactivators of Protein Arginine Deiminase 4: Functional and Structural Characterization. *Biochemistry* **45**, 11727–11736 (2006).

29. Maiuri, M. C., Zalckvar, E., Kimchi, A. & Kroemer, G. Self-eating and self-killing: crosstalk between autophagy and apoptosis. *Nature Reviews Molecular Cell Biology* **8**, 741–752 (2007).
30. Maiuri, M. C. *et al.* Stimulation of autophagy by the p53 target gene Sestrin2. *Cell Cycle* **8**, 1571–1576 (2009).
31. Budanov, A. V. & Karin, M. p53 Target Genes Sestrin1 and Sestrin2 Connect Genotoxic Stress and mTOR Signaling. *Cell* **136**, 378 (2008).
32. Brüning, A., Rahmeh, M. & Friese, K. Nelfinavir and bortezomib inhibit mTOR activity via ATF4-mediated sestrin-2 regulation. *Molecular Oncology* **7**, 1012–1018 (2013).
33. Wang, S. *et al.* ATF4 Gene Network Mediates Cellular Response to the Anticancer PAD Inhibitor YW3-56 in Triple-Negative Breast Cancer Cells. *Molecular Cancer Therapeutics* **14**, 877–888 (2015).
34. Tabas, I. & Ron, D. Integrating the mechanisms of apoptosis induced by endoplasmic reticulum stress. *Nature Cell Biology* **13**, 184–190 (2011).
35. Tohme, S., Yazdani, H., Simmons, R., Huang, H. & Tsung, A. Neutrophil extracellular traps promote the development and progression of liver metastases after surgical stress. *Cancer Research* **19**, (2017).
36. Mosmann, T. Rapid colorimetric assay for cellular growth and survival: Application to proliferation and cytotoxicity assays. *Journal of Immunological Methods* **65**, 55–63 (1983).
37. Phospho-p70 S6 Kinase (Thr389) Antibody #9205. *Cell Signaling Technology Product Datasheet* Available at: <https://www.cellsignal.com/products/primary-antibodies/phospho-p70-s6-kinase-thr389-antibody/9205>. (Accessed: 10th June 2018)

38. Hui, L., Zheng, Y., Yan, Y., Bargonetti, J. & Foster, D. A. Mutant p53 in MDA-MB-231 breast cancer cells is stabilized by elevated phospholipase D activity and contributes to survival signals generated by phospholipase D. *Oncogene* **25**, 7305–7310 (2006).
39. Ran, F. A. *et al.* Genome engineering using the CRISPR-Cas9 system. *Nature Protocols* **8**, 2281–2308 (2013).
40. Bancos, S., Baglolle, C. J., Rahman, I. & Phipps, R. P. Induction of heme oxygenase-1 in normal and malignant B lymphocytes by 15-deoxy- Δ 12,14-prostaglandin J2 requires Nrf2. *Cellular Immunology* **262**, 18–27 (2010).
41. Bansal, S., Biswas, G. & Avadhani, N. G. Mitochondria-targeted heme oxygenase-1 induces oxidative stress and mitochondrial dysfunction in macrophages, kidney fibroblasts and in chronic alcohol hepatotoxicity. *Redox Biology* **2**, 273–283 (2014).
42. Kim, K. M. *et al.* Carbon Monoxide Induces Heme Oxygenase-1 via Activation of Protein Kinase R Like Endoplasmic Reticulum Kinase and Inhibits Endothelial Cell Apoptosis Triggered by Endoplasmic Reticulum Stress. *Circulation Research* **101**, 919–927 (2007).
43. Kaplan, M. J. Role of neutrophils in systemic autoimmune diseases. *Arthritis Research & Therapy* **15**, 219 (2013).
44. Summers, C. *et al.* Neutrophil kinetics in health and disease. *Trends in Immunology* **31**, 318–324 (2010).
45. Papayannopoulos, V. Neutrophil extracellular traps in immunity and disease. *Nature Reviews Immunology* **18**, 134–147 (2017).
46. Li, Y., Guo, Y., Tang, J., Jiang, J. & Chen, Z. New insights into the roles of CHOP-induced apoptosis in ER stress. *Acta Biochimica et Biophysica Sinica* **46**, 629–640 (2014).

47. Transfecting Plasmid DNA Into MCF7 Cells Using Lipofectamine 3000 Reagent | Thermo Fisher Scientific - UK. *Thermo Fisher Scientific* Available at: <https://www.thermofisher.com/uk/en/home/references/protocols/cell-culture/transfection-protocol/mcf7-cells-protocol.html>. (Accessed: 13th July 2018)
48. Lipofectamine 3000 Reagent | Thermo Fisher Scientific - UK. *Thermo Fisher Scientific* Available at: <https://www.thermofisher.com/uk/en/home/brands/product-brand/lipofectamine/lipofectamine-3000.html>. (Accessed: 13th July 2018)
49. PADI4 peptidyl arginine deiminase 4 [Homo sapiens (human)] - Gene - NCBI. *National Center for Biotechnology Information* Available at: <https://www.ncbi.nlm.nih.gov/gene/23569#general-protein-info>. (Accessed: 22nd August 2017)
50. Lin, J.-H. *et al.* Dysregulation of HER2/HER3 Signaling Axis in Epstein-Barr Virus-Infected Breast Carcinoma Cells. *Journal of Virology* **81**, 5705–5713 (2007).
51. Sun, J. CRISPR Protocol. Unpublished Protocol. (2017).

HAONAN XU

XUHAON@GMAIL.COM

www.linkedin.com/in/haonanxu/

- EDUCATION** **The Pennsylvania State University** (University Park, PA) Aug 2014 – Aug 2018
B.S. in Chemical Engineering, Minor in Biochemistry and Molecular Biology
Schreyer Honors College; Tau Beta Pi (Engineering Honor Society)
- University College London** (London, United Kingdom) Dec 2017 – Jun 2018
Semester Abroad Program, Biological Sciences
- AWARD** Whitfield Research Endowment | Dean’s List | AIChE Freshman Recognition
- EXPERIENCE** **Researcher**, Wang Lab, Department of Biochemistry and Molecular Biology Dec 2016 – Jul 2018
- Examined cancer cell inhibition using Western Blot and other molecular biology techniques
 - Created CRISPR/Cas9 construct for generating knockout cell lines
 - Assisted on *in-vivo* cancer metastasis studies with mouse models
- Upstream Intern**, Vaccine Process Development and Commercialization, Merck & Co. May – Aug 2017
- Generated Design of Experiments to build Raman models for a yeast fermentation process
 - Constructed a scale-down model for a yeast fermentation process in 3L bioreactors
 - Authored experimental protocols, study design, and technical data packages
- Teaching Assistant**, Molecular Thermodynamics, Department of Chemistry Jan – May 2017
- Tutored statistical mechanics and thermodynamics in small groups as well as lecture settings
 - Evaluated and advised on learning progress for all students on an individual basis
- Researcher**, Curtis Lab, Department of Chemical Engineering Nov 2014 – Dec 2016
- Performed axenic extraction and symbiosis studies on more than 10 cell lines
 - Accomplished genetic transformation of 2 microalgae strains
 - Trained 3 new researchers to the level of fully autonomous
- LEADERSHIP** **Mentorship Chair**, Penn State American Institute of Chemical Engineering
- Student Program Coordinator**, Penn State Global Student Engagement Team
- International Student Orientation (ISO) Leader**, University Office of Global Programs
- PRESENTATION** **Xu H.**, Willis N., Curtis W. “Monoculture Extraction and Permeability Constraints of Hydrocarbon Producing Colony Alga *Botryococcus braunii*”. 2016 College of Engineering Research Initiative Poster Symposium, Dec 2, 2016. State College, PA.
- Cook L., Fuente P., **Xu H.**, Fodor, J., Milosavljevic B. “Photo-induced Solid State Proton Transfer from Pyranine to Hydroxyl Anion”. Department of Chemistry Poster Symposium, Apr 27, 2016. State College, PA.
- Hamaker N., Legenski K., **Xu H.**, Muzika W., Yoo J., Curtis W. “Discovery, Genome Assembly, and Interpretation of a Hydrocarbon-Producing Algae Symbiont”. 2015 AIChE Annual Conference, Nov. 8-13, 2015. Salt Lake City, UT.
- SKILL** Laboratory Western Blot, qPCR, Mammalian Cell Culture, Bioreactor/Centrifuge Scaling
- Computer MATLAB, SolidWorks, Microsoft Office, Aspen HYSYS, SnapGene, Benchling
- Language Mandarin Chinese (native fluency)